Journal of Hazardous Materials 268 (2014) 124–131

Contents lists available at ScienceDirect

Journal of Hazardous Materials

journal homepage: www.elsevier.com/locate/jhazmat

Removal of As(III) and As(V) from aqueous solutions using nanoscale zero valent iron-reduced graphite oxide modified composites

Can Wang[a,b], Hanjin Luo[a,b,*], Zilong Zhang[a,b], Yan Wu[a,b], Jian Zhang[a,b], Shaowei Chen[a,c]

[a] College of Environment and Energy, South China University of Technology, Guangzhou 510006, China
[b] The Key Lab of Pollution Control and Ecosystem Restoration in Industry Clusters, Ministry of Education, Guangzhou 510006, China
[c] Department of Chemistry and Biochemistry, University of California, Santa Cruz, CA 95064 USA

HIGHLIGHTS

- The range of applicable initial concentration is wide.
- The removal efficiencies of adsorption are rarely high.
- It is easy to separate adsorbate from adsorbent.
- The composite is more effective for As(III) than As(V).
- The residual concentration was undetected when the initial concentration of As(III) was 1 ppm.

ARTICLE INFO

Article history:
Received 29 September 2013
Received in revised form
17 December 2013
Accepted 3 January 2014
Available online 10 January 2014

Keywords:
Arsenic removal
Reduced graphite oxide
Nanoscale zero valent iron
Characteration

ABSTRACT

Nanoscale zero valent iron (NZVI) has high adsorption capacity of As(III) and As(V), but it is limited in practical use due to its small particle size and aggregation effect. Reduce graphite oxide (RGO) has been used as a support because of its high surface area. In order to utilize the advantage of NZVI and RGO as well as to avoid the disadvantage of NZVI, we loaded NZVI onto RGO via chemical reactions in this study. The adsorption capacity of As(III) and As(V), as determined from the Langmuir adsorption isotherms in batch experiments, was 35.83 mg g^{-1} and 29.04 mg g^{-1}, respectively. And the adsorption kinetics fitted well with pseudo-second-order model. The residual concentration was found to meet the standard of WHO after the samples were treated with 0.4 g L^{-1} NZVI–RGO when the initial concentration of As(III) and As(V) were below 8 ppm and 3 ppm. Especially, when the initial concentration of As(III) was below 3 ppm, the residual concentration was within 1 ppb; whereas, the residual concentration was undetected when the initial concentration of As(III) was 1 ppm.

1. Introduction

Water contamination from arsenic has been reported all over the world, and it has led to massive epidemics of arsenic poisoning in Bangladesh, West Bengal, India and other countries in South and Southeast Asia [1–4]. Arsenic is a ubiquitous, toxic and carcinogenic chemical element. And according to some reports, long terms exposure to drinking water containing arsenic causes increased occurrences of skin, lung, bladder, and kidney cancers and may even result in premature death [5]. Therefore, the World Health Organization (WHO) and some countries (such as the United States and China) had lowered the guideline for drinking water quality from 50 μg L^{-1} to 10 μg L^{-1} [6–8]. Arsenic in water primarily derived from natural (dissolution and wreathing of arsenic minerals, biological activities) and anthropogenic (industrial waste, mining, agricultural, etc.) sources [9–11]. In addition, the forms of arsenic in water are inorganic and organic, and the inorganic forms are more toxic than the organic counterparts [12]. Additionally As(III) is more toxic and difficult to be removed from water than As(V) [13,14].

As arsenic contamination is a widespread problem, many methods have been developed to remove arsenic such as adsorption [7,15–18], ion exchange [19], reverse osmosis [20,21], coagulation (coprecipitation) [22,23] and bioremediation [24,25]. Of these, adsorption is considered as a front line of defense. Nowadays a variety of absorbents have been reported for arsenic water removal, including biological materials, mineral oxides, activated carbons, and polymer resins [26–28]. Many reports indicate that nanoscale zero valent iron (NZVI) can remove a number of environmental contaminants such as lorinated solvents, organochlorine pesticides,

* Corresponding author at: College of Environmental Science and Engineering, South China University of Technology, Guangzhou 510006, Guangdong, China. Tel.: +86 20 87110517; fax: +86 20 39380508.
E-mail address: luohj@scut.edu.cn (H. Luo).

0304-3894/$ – see front matter © 2014 Elsevier B.V. All rights reserved.
http://dx.doi.org/10.1016/j.jhazmat.2014.01.009

polychlorinated biphenyls, organic dyes, and inorganic pollutants, tetracycline [29–34]. And NZVI has been considered as a promising material to remove arsenic contaminants because of its large active surface area and high arsenic adsorption capacity [35,36]. However it cannot be applied in continuous flow systems due to its small particles size and the aggregation effect. Consequently, it is necessary to load NZVI onto an appropriate support such as the activated carbon [7]. Recently, reduced graphite oxide (RGO) has received intensive attentions due to its exceptional electron transport and mechanical properties, and high surface area [37]. And the synthesis of most RGO-based multifunctional hybrid materials stems from chemically oxidized graphene oxide (GO) [38]. Moreover GO can be readily made from low-cost natural graphite in large scale. Therefore, hybrid multifunctional materials based on RGO are much more applicable than those based on pure nanomaterials. In fact, ferric hydroxide and iron oxide have been loaded to RGO or GO [39–42]. In addition, RGO is an efficient adsorbent [43,44]. Consequently, in the present study we would evaluate the use of RGO as a support to load NZVI for the removal of arsenic in water.

The objectives of this work are: (1) to prepare NZVI–RGO composites and analyze its characteristics; (2) to study the adsorption isotherms, the kinetics and the effect of initial concentration, pH, temperature and contact time; (3) to interpret the possible adsorption mechanism.

2. Experimental

2.1. Materials

All chemicals and reagents are of analyticcal grade except hydrochloric acid (HCl) which is of guaranteed reagent (GR) grade. An As(III) stock solution (1000 mg L^{-1}) was prepared by dissolving As_2O_3 in minimal amount of concentrated NaOH, and the pH was adjusted to 3.0 with concentrated HCl. The solution was then diluted to100 mL with de-ionized water. An As(V) stock solution (1000 mg L^{-1}) was prepared by using $Na_2HAsO_4{\cdot}7H_2O$ in purified water.

2.2. Preparation of GO

GO was synthesized from natural graphite (Qingdao Nanshu Ruiying Graphite Co. Ltd., China) via the Hummers method [45]. In typical reaction, graphite (5.0 g) and $NaNO_3$ (2.5 g) were added to 120 mL of concentrated H_2SO_4 (98%). And the mixture was mechanically stirred in an ice bath for 30 min. Then, $KMnO_4$ (15.0 g) was slowly added to the suspension and the temperature was kept below 5 °C for 90 min. Then the mixture was removed from the ice bath and stirred at 25–30 °C for 30 min. As the reaction progressed, the mixture gradually became pasty and the color turned into brown. Then 230 mL of de-ionized water was slowly added to the mixture and the temperature was increased to 98 °C. After stirring for 30 min, 30 mL of 30% H_2O_2 was added to the mixture, then the color of the mixture changed from brown into bright yellow. The mixture was filtered and washed with 5% HCl solution and de-ionized water several times. GO was vacuum-dried at 60 °C and obtained as brown solid.

2.3. Preparation of NZVI–RGO

To prepare NZVI-RGO hybrids, 0.5 g of GO was exfoliated into 250 mL of de-ionized water for 2 h. Then the solution was transferred to a three-neck flask and purged with N_2 for 30 min in order to remove dissolved oxygen. And 50 mL of an aqueous solution of 4.5 g $FeSO_4{\cdot}7H_2O$ in water was injected into the GO suspension slowly. The mixture was stirred constantly. After that, a $NaBH_4$ (6.0 g) aqueous solution was added to the mixture and stirred at 80 °C for 4 h. The reaction processed under the protection of N_2. The products were collected by vacuum filtration and washed several times with de-ionized water and ethanol. The resulting black solids were vacuum-dried at 60 °C. Finally, the obtained materials were stored in a N_2-purged desiccator. Ferrous iron (Fe^{2+}) was reduced according to the following reaction [46]:

$$Fe(H_2O)_6{}^{2+} + 2\,BH_4{}^- \rightarrow Fe^0\downarrow + 2\,B(OH)_3 + 7\,H_2\uparrow \quad (1)$$

2.4. Characterization

2.4.1. XRD

X-ray diffraction patterns were collected using a Bruke D8-advance X-ray diffractometer at 40 kV and 40 mA. A Cu $K\alpha$ radiation source was used. All patterns were obtained from $2\theta = 5°$ to 80° and the scanning rate was set at 0.020°/step and 17.7 s/step.

2.4.2. XPS

Surface composition to a depth of <5 nm of the nanoparticles was analyzed with a Thermo Scientific (USA) ESCALAB 250 X-ray Photoelectron Spectroscopy. All samples were dried in vacuum at room temperature and then sealed under nitrogen to avoid sample oxidation before analysis.

2.4.3. BET

RGO and NZVI–RGO were pre-dried at 60 °C in a vacuum desiccator. The samples were degassed for 6 h at 100 °C under vacuum. The surface area of RGO and NZVI–RGO particles was determined from the corresponding N_2 adsorption/desorption isotherms obtained at 77 K with an automatic instrument (ASAP2020, Micromeritics, USA).

2.4.4. TEM

TEM images were obtained using a PHILIPS (Nederland) TECNAI 10 transmission electron microscope (TEM) operated at accelerating voltage 100 kV. The GO, RGO and Fe–RGO samples were dispersed by ultrasonication before test.

2.5. Adsorption experiments

The adsorption experiments for As(III) and As(V) were performed in triplicate in a mechanical shaker at the speed of 150 rpm. Adsorption isotherms were obtained by adding 10 mg of NZVI–RGO to 25 ml of As(III) and As(V) mixture solutions with a concentration range of 1–15 ppm for 4 h at pH 7.0 (±0.25) and 25 (±0.5) °C. Adsorption kinetics were studied by batch experiments with 10 mg of NZVI–RGO were thoroughly mixed with 25 mL 7 mg L^{-1} As(III) and As(V) solutions for a predetermined time intervals (5, 15, 30, 60, 90, 120 min) at 25 (±0.5) °C and pH 7.0 (±0.25). The influence of pH on adsorption was conducted within a pH range of 2.00 to 12.00 by agitating adsorbent (10 mg) with As(III) and As(V) (25 ml, 7 ppm) for 120 min at 25 (±0.5) °C and 150 rpm. The pH was adjusted by adding aqueous solutions of 0.1 M HCl (GR) or 0.1 M NaOH and measured by the pH electrode. The influence of temperature on adsorption was studied by shaking 25 ml of 7 ppm solutions of As(III) and As(V) with 10 mg NZVI–RGO at different temperatures (15, 25, 30, 35, 45 and 55 °C), pH 7.0 (±0.25) and 150 rpm for 120 min.

The suspensions were filtered through a 0.45 μm membrane filter and the concentration of arsenic was quantified. The initial and residual concentrations of arsenic were determined with an 830 atomic fluorescence spectrophotometer (AFS). The specific amount of arsenic adsorbed was calculated from the following equation:

$$q_e = \frac{V\,(C_o - C_e)}{m} \quad (1)$$

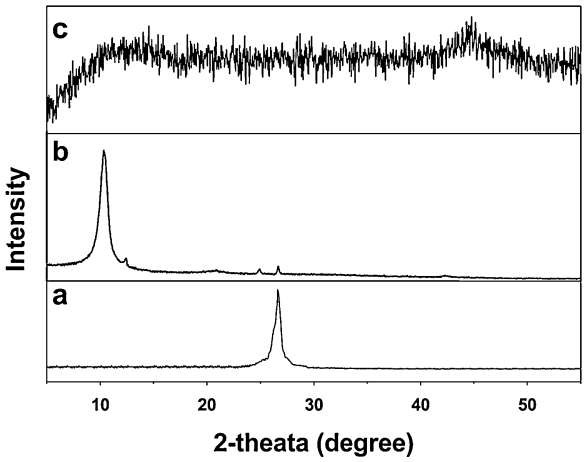

Fig. 1. (a) X-ray diffraction analysis of graphite (b) X-ray diffraction analysis of GO. (c) X-ray diffraction analysis of NZVI–RGO.

where C_o is the initial concentration ($mg\,L^{-1}$), C_e is the equilibrium concentration ($mg\,L^{-1}$), q_e is the amount of As adsorbed on NZVI–RGO at equilibrium ($mg\,g^{-1}$), V is the solution volume (L), and m is the mass of the adsorbent (g).

2.6. As analysis

An 830 atomic fluorescence spectrophotometer (Beijing Jitian Instrument Company, China) was used for the determination of the arsenic concentration. It was coupled with a hollow double cathode arsenic lamp. To detect As(III) selectively, the working solution was prepared with a mixture of 2% $NaBH_4$ and 0.5% NaOH as the reducing solution and 5% HCl (GR) as the carrier solution. The total lamp current and auxiliary lamp current for arsenic analysis were set at 60 and 30 mA, respectively. The height of the atomizer was fixed at 11 mm and the voltage of the instrument was 270 V. Argon (99.999%) was used as the carrier gas and shielding gas and the flow rate was set to 300 mL min^{-1} and 700 mL min^{-1}, respectively. The speed of the pump was 100 rar min^{-1}. Under this condition, only As(III) was converted to AsH_3 and detected by the AFS instrument. The correlation coefficient of the standard curve ($n = 5$) was greater than 0.998. And the detection limit of the instrument was 0.01 $\mu g\,L^{-1}$.

3. Results and discussion

3.1. Characterizations of adsorbents

Fig. 1 shows the XRD patterns of graphite, GO and NZVI–RGO. Graphite (Fig. 1a) exhibits a sharp peak at 26.64° corresponding to an interlayer distance of 0.334 nm. After oxidation, this peak weakened and there is a new peak at 10.36°, corresponding to an interlayer spacing of 0.853 nm, which is ascribed to the presence of abundant oxygen containing functional groups on the surfaces of the GO sheets [47]. From Fig. 1c, the peak of GO disappeared and there was a weak and broad peak at 44.63°, which suggested that the GO was reduced by the sodium borohydride and zero-valent of iron (Fe^0) was loaded to the RGO sheets [31,34,48]. And the results were further supported by the XPS measurements.

The wide XPS spectra before (NZVI–RGO) and after reaction with As(III) and As(V) show photo electron lines at a binding energy of about 284.82, 530.59, 711.3, 192.25 and 45.4 eV, which may be attributed to C 1s, O 1s, Fe 2p, B 1s and As 3d, respectively (Fig. 2a). Deconvolution of the C 1s peak (Fig. 2b1 and b2) of GO and NZVI–RGO shows three peaks at about 284.8, 286.05, and 287.8 and 289.0 eV, corresponding to C–C, C–O, C=O and O–C=O groups [49,50], respectively. From the (Fig. 2 b1and b2), we can know the C 1s spectra of NZVI–RGO show mainly the C–C and C–O, which suggests that the GO can be reduced by sodium borohydride effectively. In the spectrum of Fe 2p (Fig. 2c), the peaks at Fe $2p_{3/2}$ and Fe $2p_{1/2}$ are located at 710.68 and 724.57 eV for γ-Fe_2O_3 [51,52]. In addition, the satellite peak at 719.81 eV is characteristic of γ-Fe_2O_3 [52]. Furthermore, a feature peak of Fe(0) [31] can be found at around 706.69 eV, suggesting that Fe^0 does exist on the RGO surface. The results suggest that the forms of Fe on the composite surface are γ-Fe_2O_3 and Fe(0). After the reaction, the peak of Fe(0) could not be found and the peak intensity for Fe(III) and Fe(II) increased, showing that Fe^0 had been oxidized on the surface of NZVI–RGO. Fig. 2a shows a full survey of the surface composition before and after the reaction with As(III) and As(V), and the samples after reaction showed a peak at 45.45 eV which is the feature peak of arsenic and indicates that the arsenic was absorbed by the NZVI–RGO. Fig. 2d shows the XPS spectra of the sample treated with As(III) and As(V). The As(III) treated sample shows two peaks at 44.25 and 41.5 eV, corresponding to As(III) and As(0), respectively. And the XPS spectra of the sample treated with As(V) shows only one peak at 45.5 eV, corresponding to the characteristic peak of the As(V). The result is similar to that reported by Bang et al. [53].

According to the method of the supplementary material [54], the structure of the RGO was significantly altered after loading nano zero-valent iron (66.45%). The surface area of the RGO and NZVI–RGO were measured by a BET analyzer, and the surface area of the samples was calculated to be 147.58 and 100.65 $m^2\,g^{-1}$. The surface area of NZVI–RGO decreased with the NZVI loaded onto RGO. The result is similar to reports of some literatures [39,55].

Fig. 3 shows the TEM images of GO (a) and NZVI–RGO (b1 and b2) composites samples. From Fig. 3a, the graphene sheets were found obviously and folding nature can be observed clearly. In Fig. 3b1 and b2, NZVI can be observed obviously which suggested that they are loaded to the GO sheet and the particle size is about 40 nm. It is dispersed homogeneously and predominantly than pure NZVI [29] but there is still agglomeration. It is well known that the NZVI will be agglomerated seriously and appeared as bulkier acerate or dendritic flocs without any dispersing agent [29]. These observations suggest that the RGO has the effect of a dispersing agent.

3.2. Adsorption isotherm study

Adsorption isotherms can explain the relationship between adsorbate and adsorbent and provide the parameter for designing a desired adsorption method. The Langmuir [56] and Freundlich [57] isotherm models are applied to simulate As(III)and As(V) adsorption on NZVI–RGO. The Langmuir model can be expressed as:

$$\frac{C_e}{q_e} = \frac{C_e}{q_m} + \frac{1}{k_l q_m} \tag{2}$$

The Freundlich isotherm model can be expressed by the following formula:

$$q_e = k_f \sqrt[n]{C_e} \tag{3}$$

or:

$$lgq_e = \frac{1}{n} lgC_e + lgk_f \tag{4}$$

where q_m ($mg\,g^{-1}$) represents the maximum adsorption capacity and k_l ($L\,mg^{-1}$) is the Langmuir constant, which represents the affinity between the solute and adsorbent. The Freundlich constant (k_f) is the parameter, and ($1/n$) is the adsorption intensity ($1 < n < 10$).

The results of adsorption isotherms are listed in Fig. 4 and the relative parameters calculated from the two models are listed in

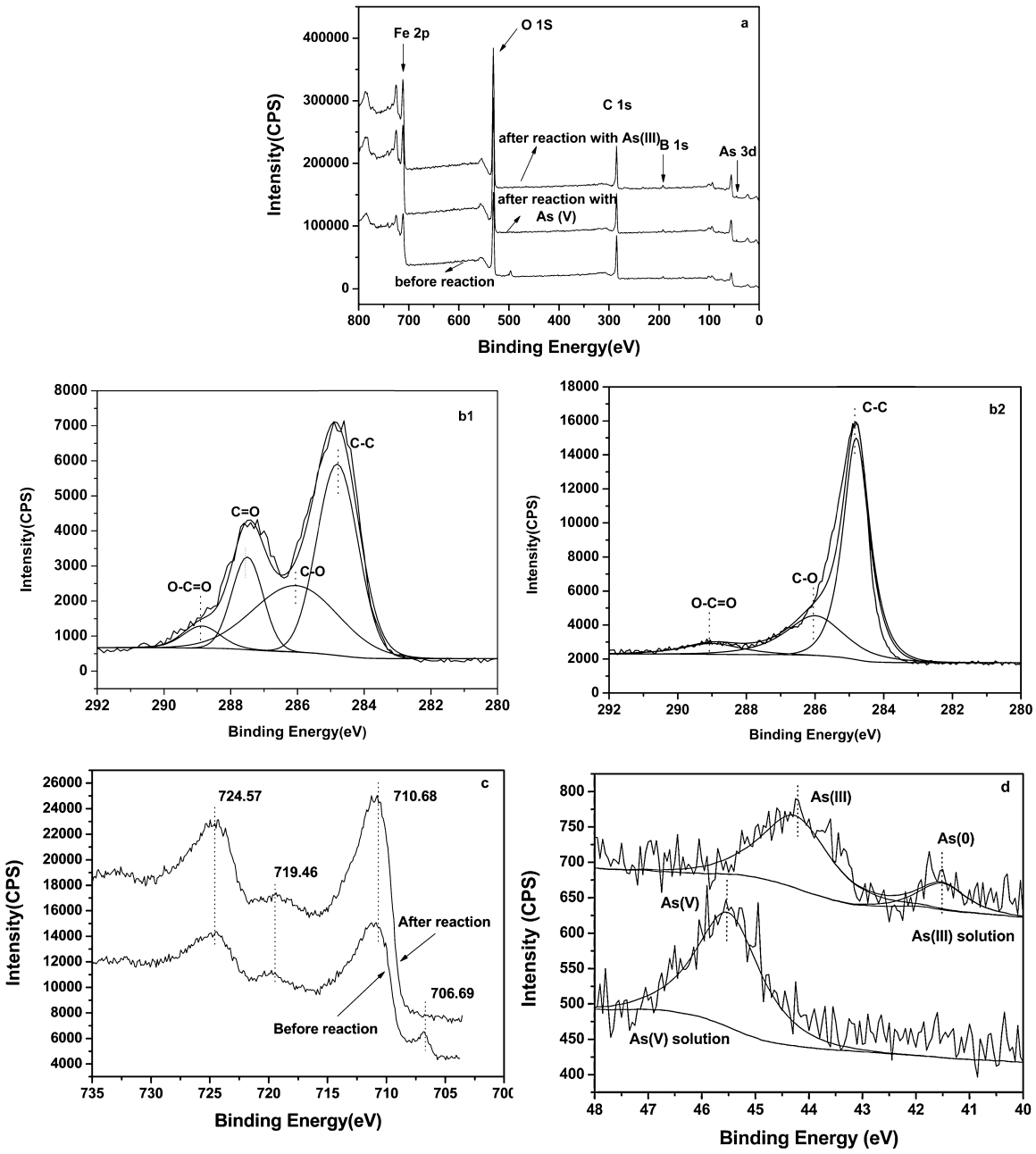

Fig. 2. XPS response of (a) full survey of before and after reaction with As(III) and As(V); (b) C 1s core levels of RGO (b1) and NZVI–RGO (b2); (c) Fe 2p core levels of before and after reaction; (d) As 3d core levels of after reaction with As(III) and As(V).

Table 1. The higher correlation coefficient of the Langmuir model indicates that the adsorption data are better fitted by the Langmuir model ($R^2 > 0.995$) than the Ferundlich model ($R^2 > 0.87$). This means, that the adsorption involved the formation of a monolayer on a homogeneous surface. Moreover the Freundlich constant for n was found higher than 2.70, indicating the adsorption of arsenic on NZVI–RGO was a favorable process. It can be found from Table 1 that the maximum adsorption capacities obtained for NZVI–RGO with As(III) and As(V) was 35.83 mg g^{-1} and 29.04 mg g^{-1}, which is much higher than that of Fe_3O_4–RGO–MnO_2 composites, Fe_3O_4–RGO [39,55] and NZVI/AC [7]. Furthermore, from Fig. 5 it can be seen that the residual total concentration of As(III) met the standard for drinking water (10 ppb) when the initial As(III) concentration was less than 8 mg L^{-1} and the initial As(V) concentration was less than 3 mg L^{-1} and the samples were treated by NZVI–RGO composites with a dosage at 0.4 g L^{-1}. In addition, the residual total concentration was not detectable by the instrument when the initial concentration of As(III) was only 1 ppm. Compared with other adsorbents in Table 2, the adsorption capacity of NZVI–RGO is a new composite material which is more effective and evident than

Table 1
Langmuir and Freundlich adsorption isotherm parameters for As(III) and As(V) adsorption on NZVI–RGO at pH 7.0(±0.25) and 25(±0.5) °C.

	As(III)	As(V)
Langmuir		
q_m(mg g^{-1})	35.83	29.04
k_l(L mg^{-1})	132.9	19.33
R^2	0.9988	0.9955
Freundlich		
n	5.230	2.730
k_f	38.67	35.56
R^2	0.9208	0.8753

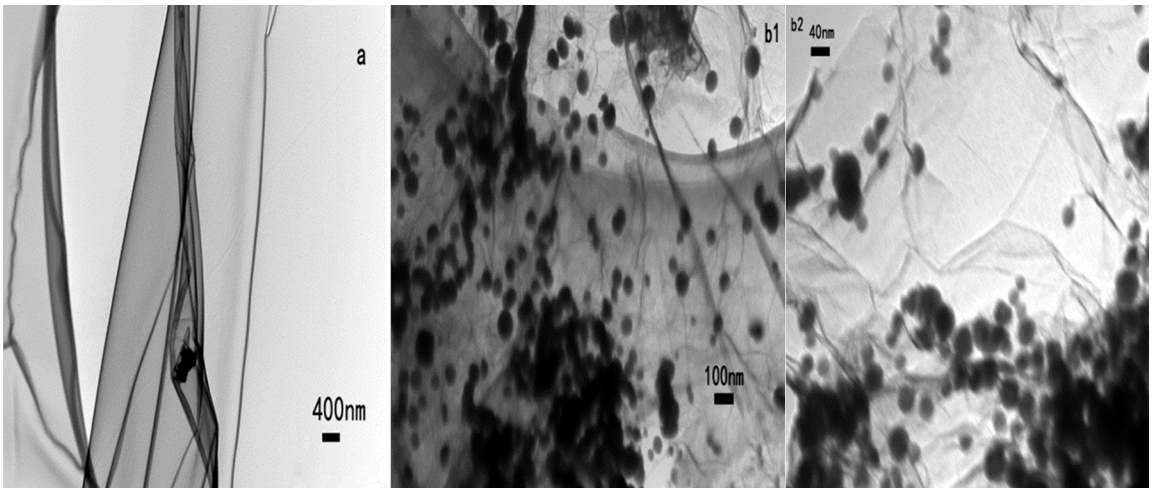

Fig. 3. (a) TEM image of the synthesized GO; (b1 and b2) TEM images of the NZVI–RGO.

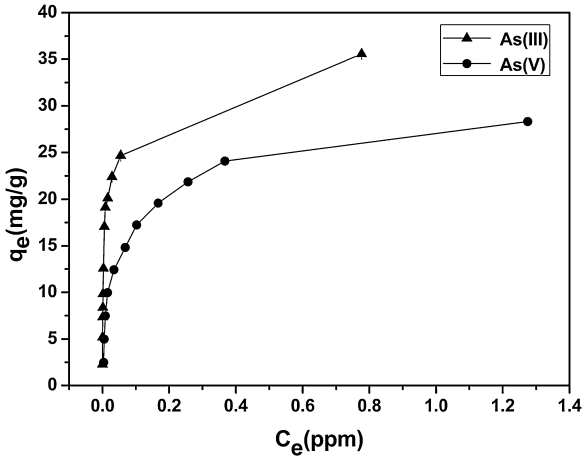

Fig. 4. Adsorption isotherm parameters for As(III) and As(V) adsorption on NZVI–RGO at pH 7.0 (±0.25) and 25 (±0.5) °C.

those reported in the literature. The dose of NZVI–RGO is only 0.4 g L^{-1}, and it is less than some materials, such as the NZVI–AC [7] (1.0 g L^{-1}), NZVI [36] (1.0 g L^{-1}), and the others [54,58–61]. And the range of initial concentration is rarely broad. As the adsorbent exhibited strong affinity to As(III) and As(V) and it is friendly to the environment and non-poisonous to human being, it served as a more efficient adsorbent in drinking water treatment in the future. But the reusability and the mechanism have to be studied in the future.

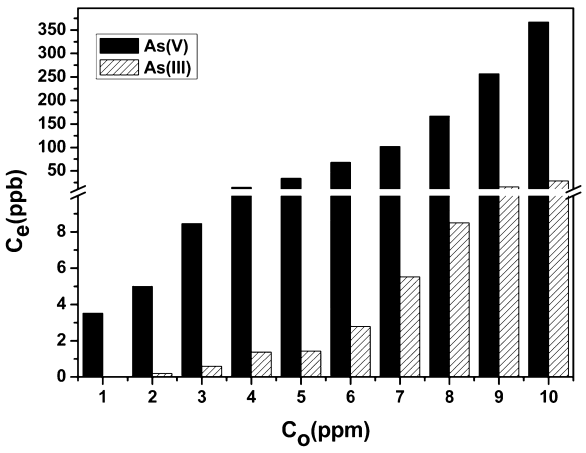

Fig. 5. The contrast of equilibrium concentration and the standard of WHO with different initial concentration.

3.3. Adsorption kinetics

In ordered to describe the adsorption rate, the pseudo-first-order kinetics model [62] and the pseudo-second-order kinetics model [63] were employed in this study. The linearized-integral forms are as follows, respectively:

$$\lg(q_e - q_t) = \lg\ q_e - \frac{k_1 t}{2.303}, \tag{5}$$

$$\frac{t}{q_t} = \frac{1}{2}k_2 q_e^2 + \frac{t}{q_e} \tag{6}$$

$$V_0 = k_2 q_e^2$$

where q_e (mg g^{-1}) and q_t (mg g^{-1}) are the adsorption capacity at equilibrium time and at time t (min), k_1 (min^{-1}) and k_2 (g mg^{-1} min^{-1}) are the pseudo-first-order adsorption rate constant and the pseudo-second-order adsorption rate constant, respectively, and V_0 (mg g^{-1} min^{-1}) is the pseudo-second-order adsorption initial rate (at t = 0 min). Therefore, the V_0 and q_e values of kinetic tests can be determined experimentally by plotting the t/q_t versus t.

The fitting results of the adsorption kinetics are listed in Fig. 6 and Table 3. From Fig. 6a, the equilibrium time was found within 30 and 60 min and thus we selected 60 min as the optimum equilibrium time which is shorter than that with carbon-based adsorbents. In addition, the adsorption process was rapid within the first 30 min for both As(III) and As(V), then slowly down, suggesting that the adsorption process involved two stages, namely, surfaces adsorption and inter adsorption in layer graphene between adsorbate and adsorbent. Moreover it can be seen from the calculated (cal) parameters that the pseudo-second-order kinetic model is a better fit to the experimental (exp) data than the pseudo-first-order kinetic model, and the coefficients of determination R^2 is higher than the pseudo-first-order kinetic model. Consequently, the results of adsorption kinetics indicate that As(III) and As(V) uptake on NZVI–RGO is followed the pseudo-second-order kinetic model. It is different from some reports about the adsorption of the As(III) and As(V) on NZVI [36,64] and the NZVI/AC [7] which they are fitted to a pseudo-first-order reaction kinetics and the Boyd model. But it is similar to the adsorbent which are the RGO as the support

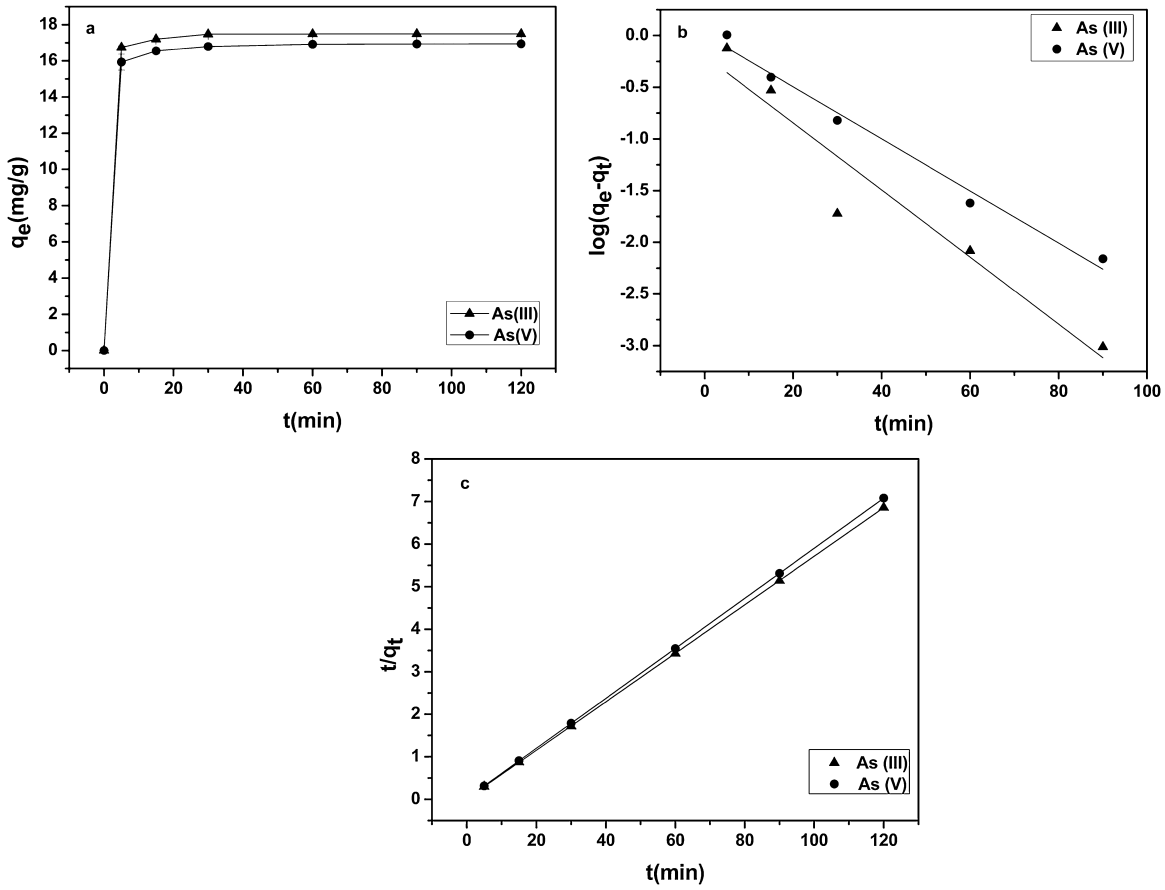

Fig. 6. Adsorption kinetic parameters for As(III) and As(V) on NZVI–RGO at pH 7.0 (±0.25) and 25(±0.5) °C. (As(III) and As(V) initial concentration with 7 mg/L) (a) the concentration of arsenic at some interval time; (b) the pseudo-first-order kinetics model data for As(III) and As(V), respectively; (c) the pseudo-second-order kinetics model data for As(III) and As(V), respectively.

Table 2
Comparison As(III) and As(V) adsorption capacity (q_m, mg g^{-1}) with some adsorbent materials in the references.

Adsorbent	pH	Concentration range (ppm)	Adsorption capacity (mg g^{-1})		Reference
			As(III)	As(V)	
NZVI–RGO nanoparticles	7	1–10	35.83	29.04	This paper
NZVI-actived carbon nanoparticles	7	2	18.2	12.0	[7]
NZVI nanoparticles	7		3.5	–	[36]
Iron-containing ordered mesoporous carbon	6.5	1–24	9.3	7.0	[61]
Fe_3O_4–RGO nanoparticles	7	3–7	13.1	10.2	[39]
Fe_3O_4–RGO–MnO_2 nanoparticles	7	0.01–10	14.04	12.22	[55]
Magnetite nanoparticles	2	2	3.7	3.7	[70]

[39,55]. Now the transformations and translocation of arsenic at and within the nanoparticles are not are not clearly Ramos et al. [65] reported that reduction As(III) or As(V) species to elemental arsenic by nZVI was an important mechanism for arsenic immobilization. And Yan et al. [59] observed that As(III) species undergo two stages of transformation upon adsorption at the nZVI surface. The first stage is breaking of As–O bonds at nZVI surface, and the second stage involves further reduction and diffusion of arsenic across the thin oxide layer enclosing the nanoparticles. Therefore, especially our material is nZVI–RGO and it is more complex than nZVI, so now we are contributing to research the mechanism.

3.4. Effect of temperature

From Fig. 7, it can be seen that the removal increased when the temperature was increased from 15 to 25 °C. Similar results were reported previously [66]. However the removal of arsenic decreased when the temperature was increased further, the

Table 3
Parameters of the pseudo first-order and second-order kinetic models for the adsorption of As(III) and As(V) on the NZVI–RGO, respectively.

	Exp	Pseudo-first-order			Pseudo-second-order			
	q_e,exp	k_1	q_e, cal1	R^2	k_2	q_e, cal2	V_0	R^2
As(III)	17.498	0.951	0.638	0.672	7.5×10^{-5}	17.535	0.02312	0.999
As(V)	17.150	0.986	1.022	0.839	1.44×10^{-4}	17.001	0.04174	0.999

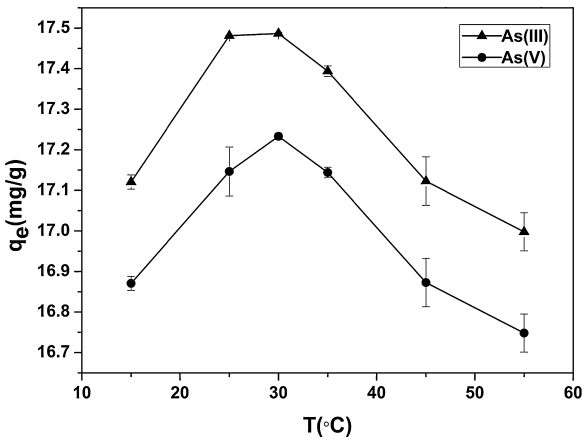

Fig. 7. Effect of temperature for As(III) and As(V) adsorption on NZVI–RGO nanocomposites at pH 7.0 (±0.25), initial As(III) and As(V) concentration is 7 mg/L, respectively.

literature of Partey et al. [67] has the similar results. Therefore, the temperature of the maximum arsenic ions adsorption is about 30 °C. Unfortunately, we cannot found the reason for this result. Some reports said that the mobility of ions will increase when the temperature increased. And the surface complexation and the electrostatic interactions may decrease when the temperature is above 30 °C.

3.5. Effect of pH

The effect of pH on the adsorption ratio of As(V) and As(III) is illustrated in Fig. 8. The adsorption capacity of NZVI–RGO is optimal when the pH ranges from 4 to 10. As we all know the species of ions in an aqueous solution is mainly determined by the pH and the dissociation constants. The dissociation constants of aqueous As(V) are $pK_{a1} = 2.1$, $pK_{a2} = 6.7$, $pK_{a3} = 11.2$, consequently the As(V) is present as $H_2AsO_4^-$, $HAsO_4^{2-}$ and AsO_4^{3-} when pH is changed from 2 to 12 and all of them are negative anions [28,68]. In comparison, the dissociation constants of aqueous As(III) are $pK_{a1} = 9.1$, $pK_{a2} = 12.1$ and $pK_{a3} = 13.4$, and the species of As(III) mainly includes neutral H_3AsO_3 (pH < 9.1) and anionic $H_2AsO_3^-$ (9.1 < pH < 12.1) [28,68]. Moreover, the pH point of zero charge (pH_{PZC}) is an important factor, and the pH_{PZC} of NZVI–RGO is 7.5. It is well known that a solid surface is positively charged when the pH is below the pH_{PZC}, and negatively charged when the pH is above the pH_{PZC}. Therefore, from Fig. 8 when the pH is below pH_{PZC}, the surface of the composite adsorbent is positively charged, it attracts large of the anionsic As(V) at low pH. With the increase of pH, the adsorbent became less positively charged, and the adsorption of As(V) decreased significantly. That is, the method of absorption with As(V) is controlled by the electrostatic interactions. Similar results were also obtained by Zhu et al. [7,28,39,55]. In contrast, at pH < 9.1, As(III) is primarily in the form of neutral H_3AsO_3, and the increase in the adsorption of As(III) in alkaline solutions, which suggests that the electrostatic factors do not control the adsorption onto NZVI–RGO. According some previous research [36,69], the As(III) adsorption reaction forms on ZVI corrosion reaction forms is complexes. The increase of adsorption with As(III) suggests that the method is controlled by surface complexation, there are some previous literatures have similar results [7,36,39].

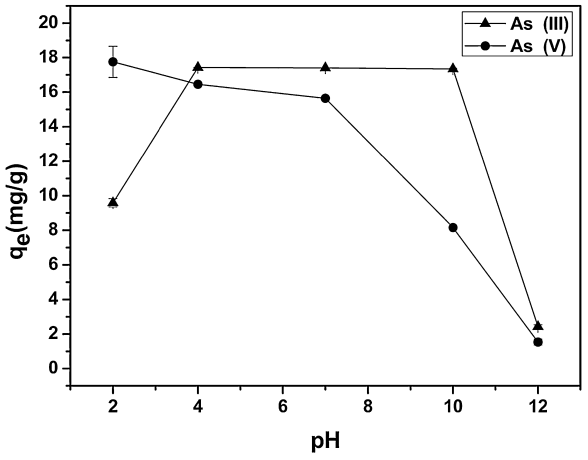

Fig. 8. Effect of pH for As(III) and As(V) adsorption on NZVI-RGO nanocomposites at 25 (±0.5) °C, initial As(III) and As(V) concentration is 7 mg/L, respectively.

Therefore, the mechanisms of adsorption with As(V) and As(III) are different, the adsorption of As(III) is divided into two processes, surface complexation(pH < 9.1) and electrostatic interactions (pH > 9.1). The similar results could be obtained by the literatures of Chandra and Zhu et al. [7,39].

4. Conclusions

The present study suggests that the NZVI–RGO hybrids are promising and effective composite for the removal of As(III) and As(V) in wastewater. The adsorption capacity varies with different conditions. The optimal temperature is about 30 °C. pH is another significant factor affecting the removal efficiency of As(III) and As(V) by NZVI–RGO. The optimal pH for the removal of As(V) is about 2, however the optimal pH for the removal of As(III) ranges from 4 to 10. The adsorption capacity of As(III) and As(V) from the Langmuir adsorption isotherms in batch experiments were 35.83 mg g^{-1} and 29.04 mg g^{-1}, respectively. The residual concentration after the samples were treated by 0.4 g L^{-1} met the standard of WHO concentration when the initial concentration of As(V) and As(III) were 8 ppm and 3 ppm, respectively. Especially, the residual concentration is below 1 ppb when the initial concentration of As(III) is below 3 ppm, and the residual concentration was not detectable by the instrument when the initial concentration of As(III) below 1 ppm.

Acknowledgements

This work is financially supported by National Natural Science Foundation of China (No. 40973074) and the National High Technology Research and Development Program of China (2013AA06A209) for financial support.

Appendix A. Supplementary data

Supplementary data associated with this article can be found, in the online version, at http://dx.doi.org/10.1016/j.jhazmat.2014.01.009.

References

[1] P.F. Souter, et al., Evaluation of a new water treatment for point-of-use household applications to remove microorganisms and arsenic from drinking water, Journal of Water and Health 1 (2) (2003).
[2] P. Bagla, J. Kaiser, India's spreading health crisis draws global arsenic experts, Science (New York, NY) 274 (1996) 5285.
[3] A.H. Smith, E.O. Lingas, M. Rahman, Contamination of drinking-water by arsenic in Bangladesh: a public health emergency, Bulletin of the World Health Organization 78 (9) (2000) 1093–1103.
[4] M. Berg, et al., Arsenic contamination of groundwater and drinking water in Vietnam: a human health threat, Environmental Science and Technology 35 (13) (2001) 2621–2626.

[5] M.N. Bates, A.H. Smith, C. Hopenhayn-Rich, Arsenic ingestion and internal cancers: a review, American Journal of Epidemiology 135 (5) (1992).
[6] M.J. Abedin, J. Cotter-Howells, A.A. Meharg, Arsenic uptake and accumulation in rice (*Oryza sativa* L.) irrigated with contaminated water, Plant and Soil 240 (2) (2002) 311–319.
[7] H.J. Zhu, et al., Removal of arsenic from water by supported nano zero-valent iron on activated carbon, Journal of Hazardous Materials 172 (2–3) (2009) 1591–1596.
[8] WHO, Guidelines for drinking water quality Recommendations, 1, second ed., World Health Organization, Geneva, 1993.
[9] R.S. Oremland, J.F. Stolz, The ecology of arsenic, Science 300 (5621) (2003) 939–944.
[10] A.H. Welch, et al., Arsenic in ground water of the United States: occurrence and geochemistry, Groundwater 38 (4) (2000) 589–604.
[11] P.L. Smedley, D.G. Kinniburgh, A review of the source, behaviour and distribution of arsenic in natural waters, Applied Geochemistry 17 (5) (2002) 517–568.
[12] R.A. Yokel, S.M. Lasley, D.C. Dorman, The speciation of metals in mammals influences their toxicokinetics and toxicodynamics and therefore human health risk assessment, Journal of Toxicology and Environmental Health—Part B—Critical Reviews 9 (1) (2006) 63–85.
[13] F.C. Knowles, A.A. Benson, The Biochemistry of Arsenic, Trends in Biochemical Sciences 8 (5) (1983) 178–180.
[14] N.E. Korte, Q. Fernando, A review of arsenic (III) in groundwater, Critical Reviews in Environmental Science and Technology 21 (1) (1991) 1–39.
[15] A. Sperlich, et al., Breakthrough behavior of granular ferric hydroxide (GFH) fixed-bed adsorption filters: modeling and experimental approaches, Water Research 39 (6) (2005) 1190–1198.
[16] Q.L. Zhang, et al., A method for preparing ferric activated carbon composites adsorbents to remove arsenic from drinking water, Journal of Hazardous Materials 148 (3) (2007) 671–678.
[17] K.J. Reddy, K.J. McDonald, H. King, A novel arsenic removal process for water using cupric oxide nanoparticles, Journal of Colloid and Interface Science 397 (2013) 96–102.
[18] X.L. Wu, et al., Water-dispersible magnetite–graphene–LDH composites for efficient arsenate removal, Journal of Materials Chemistry 21 (43) (2011) 17353–17359.
[19] J. Kim, M.M. Benjamin, Modeling a novel ion exchange process for arsenic and nitrate removal, Water Research 38 (8) (2004) 2053–2062.
[20] I. Akin, et al., Removal of arsenate [As(V)] and arsenite [As(III)] from water by SWHR and BW-30 reverse osmosis, Desalination 281 (2011) 88–92.
[21] R.Y. Ning, Arsenic removal by reverse osmosis, Desalination 143 (3) (2002) 237–241.
[22] A. Zouboulis, I. Katsoyiannis, Removal of arsenates from contaminated water by coagulation-direct filtration, Separation Science and Technology 37 (12) (2002) 2859–2873.
[23] M.B. Baskan, A. Pala, A statistical experiment design approach for arsenic removal by coagulation process using aluminum sulfate, Desalination 254 (1–3) (2010) 42–48.
[24] T.M. Gihring, et al., Rapid arsenite oxidation by *Thermus aquaticus* and *Thermus thermophilus*: field and laboratory investigations, Environmental Science and Technology 35 (19) (2001) 3857–3862.
[25] E.O. Omoregie, et al., Arsenic bioremediation by biogenic iron oxides and sulfides, Applied and Environmental Microbiology 79 (14) (2013).
[26] M.M. Benjamin, et al., Sorption and filtration of metals using iron-oxide-coated sand, Water Research 30 (11) (1996) 2609–2620.
[27] L. Dambies, T. Vincent, E. Guibal, Treatment of arsenic-containing solutions using chitosan derivatives: uptake mechanism and sorption performances, Water Research 36 (15) (2002) 3699–3710.
[28] D. Mohan, C.U. Pittman, Arsenic removal from water/wastewater using adsorbents—a critical review, Journal of Hazardous Materials 142 (1–2) (2007) 1–53.
[29] H. Chen, et al., Removal of tetracycline from aqueous solutions using polyvinylpyrrolidone (PVP-K30) modified nanoscale zero valent iron, Journal of Hazardous Materials 192 (1) (2011) 44–53.
[30] F. He, D.Y. Zhao, Manipulating the size and dispersibility of zerovalent iron nanoparticles by use of carboxymethyl cellulose stabilizers, Environmental Science and Technology 41 (17) (2007) 6216–6221.
[31] Y.P. Sun, et al., A method for the preparation of stable dispersion of zero-valent iron nanoparticles, Colloids and Surfaces A—Physicochemical and Engineering Aspects 308 (1–3) (2007) 60–66.
[32] L.J. Kecskes, R.H. Woodman, S.F. Trevino, B.R. Klotz, S.G. Hirsch, B.L. Gersten, Characterization of a nanosized iron powder by comparative methods, Kona 21 (2003) 143–150.
[33] D. Karabelli, et al., Batch removal of aqueous Cu^{2+} ions using nanoparticles of zero-valent iron: a study of the capacity and mechanism of uptake, Industrial and Engineering Chemistry Research 47 (14) (2008) 4758–4764.
[34] A. Giasuddin, S.R. Kanel, H. Choi, Adsorption of humic acid onto nanoscale zerovalent iron and its effect on arsenic removal, Environmental Science and Technology 41 (6) (2007) 2022–2027.
[35] B.K. Mandal, et al., Synthesis of zero valent iron nanoparticles and application to removal of arsenic(III) and arsenic(V) from water, Journal of the Indian Chemical Society 89 (9) (2012) 1215–1221.
[36] S.R. Kanel, et al., Removal of arsenic(III) from groundwater by nanoscale zero-valent iron, Environmental Science and Technology 39 (5) (2005) 1291–1298.
[37] H. Kim, A.A. Abdala, C.W. Macosko, Graphene/polymer nanocomposites, Macromolecules 43 (16) (2010) 6515–6530.
[38] S. Stankovich, et al., Synthesis of graphene-based nanosheets via chemical reduction of exfoliated graphite oxide, Carbon 45 (7) (2007) 1558–1565.
[39] V. Chandra, et al., Water-dispersible magnetite-reduced graphene oxide composites for arsenic removal, ACS Nano 4 (7) (2010) 3979–3986.
[40] K. Zhang, et al., Graphene oxide/ferric hydroxide composites for efficient arsenate removal from drinking water, Journal of Hazardous Materials 182 (1-3) (2010) 162–168.
[41] W. Xi-Lin, et al., Water-dispersible magnetite–graphene–LDH composites for efficient arsenate removal, Journal of Materials Chemistry 21 (43) (2011) 17353–17359.
[42] H. Jabeen, et al., Enhanced Cr(VI) removal using iron nanoparticle decorated graphene, Nanoscale 3 (9) (2011) 3583–3585.
[43] Q. Liu, et al., Evaluation of graphene as an advantageous adsorbent for solid-phase extraction with chlorophenols as model analytes, Journal of Chromatography A 1218 (2) (2011) 197–204.
[44] Y. Wu, et al., Adsorption of hexavalent chromium from aqueous solutions by graphene modified with cetyltrimethylammonium bromide, Journal of Colloid and Interface Science 394 (2013) 183–191.
[45] W.S. Hummers, R.E. Offeman, Preparation of graphitic oxide, Journal of the American Chemical Society 1958 (80) (1939).
[46] C.B. Wang, W.X. Zhang, Synthesizing nanoscale iron particles for rapid and complete dechlorination of TCE and PCBs, Environmental Science and Technology 31 (7) (1997) 2154–2156.
[47] Y.X. Xu, et al., Flexible graphene films via the filtration of water-soluble noncovalent functionalized graphene sheets, Journal of the American Chemical Society 130 (18) (2008) 5856–5857.
[48] Y.P. Sun, et al., Characterization of zero-valent iron nanoparticles, Advances in Colloid and Interface Science 120 (1-3) (2006) 47–56.
[49] Z.S. Wu, et al., Synthesis of high-quality graphene with a pre-determined number of layers, Carbon 47 (2) (2009) 493–499.
[50] X.Y. Peng, et al., Synthesis of electrochemically-reduced graphene oxide film with controllable size and thickness and its use in supercapacitor, Carbon 49 (11) (2011) 3488–3496.
[51] J. Lu, et al., Solvothermal synthesis and characterization of Fe_3O_4 and gamma-Fe_2O_3 nanoplates, Journal of Physical Chemistry C 113 (10) (2009) 4012–4017.
[52] D.H. Zhang, et al., Magnetite (Fe_3O_4) core-shell nanowires: synthesis and magnetoresistance, Nano Letters 4 (11) (2004) 2151–2155.
[53] S. Bang, et al., Chemical reactions between arsenic and zero-valent iron in water, Water Research 39 (5) (2005) 763–770.
[54] Z.M. Gu, J. Fang, B.L. Deng, Preparation and evaluation of GAC-based iron-containing adsorbents for arsenic removal, Environmental Science and Technology 39 (10) (2005) 3833–3843.
[55] X.B. Luo, et al., Adsorption of As(III) and As(V) from water using magnetite Fe_3O_4-reduced graphite oxide-MnO_2 nanocomposites, Chemical Engineering Journal 187 (2012) 45–52.
[56] I. Langmuir, Adsorption of gases on glass, mica and platinum, Journal of America Chemistry Society 40 (9) (1918) 1361–1403.
[57] H.M.F.Z. Freundlich, Stoechiometrie und Verwandtschaftslehre, Zeitschrift fuer Physikalische Chemie (1906) 385–470.
[58] N. Sahiner, et al., Arsenic(V) removal with modifiable bulk and nano *p*(4-vinylpyridine)-based hydrogels: the effect of hydrogel sizes and quarternization agents, Desalination 279 (1–3) (2011) 344–352.
[59] W. Yan, et al., Intraparticle reduction of arsenite (As(III)) by nanoscale zerovalent iron (nZVI) investigated with in situ X-ray absorption spectroscopy, Environmental Science and Technology 46 (13) (2012) 7018–7026.
[60] M.A. Barakat, N. Sahiner, Cationic hydrogels for toxic arsenate removal from aqueous environment, Journal of Environmental Management 88 (4) (2008) 955–961.
[61] Z.M. Gu, B.L. Deng, J. Yang, Synthesis and evaluation of iron-containing ordered mesoporous carbon (FeOMC) for arsenic adsorption, Microporous and Mesoporous Materials 102 (1–3) (2007) 265–273.
[62] M. Dogan, et al., Adsorption kinetics of maxilon blue GRL onto sepiolite from aqueous solutions, Chemical Engineering Journal 124 (1–3) (2006) 89–101.
[63] Y.S. Ho, Review of second-order models for adsorption systems, Journal of Hazardous Materials 136 (3) (2006) 681–689.
[64] S.R. Kanel, J.M. Greneche, H. Choi, Arsenic(V) removal kom groundwater using nano scale zero-valent iron as a colloidal reactive barrier material, Environmental Science and Technology 40 (6) (2006) 2045–2050.
[65] M. Ramos, et al., Simultaneous oxidation and reduction of arsenic by zero-valent iron nanoparticles: understanding the significance of the core–shell structure, Journal of Physical Chemistry C 113 (33) (2009) 14591–14594.
[66] D. Pokhrel, T. Viraraghavan, Arsenic removal from an aqueous solution by modified A-niger biomass: batch kinetic and isotherm studies, Journal of Hazardous Materials 150 (3) (2008) 818–825.
[67] F. Partey, et al., Arsenic sorption onto laterite iron concretions: temperature effect, Journal of Colloid and Interface Science 321 (2) (2008) 493–500.
[68] A. Ringbom, Complexation in Analytical Chemistry, Interscience–Wiley, New York, NY, 1963.
[69] B.A. Manning, et al., Arsenic(III) and arsenic(V) reactions with zerovalent iron corrosion products, Environmental Science and Technology 36 (24) (2002) 5455–5461.
[70] A.I. Zouboulis, I.A. Katsoyiannis, Recent advances in the bioremediation of arsenic-contaminated groundwaters, Environment International 31 (2) (2005) 213–219.